HELIOGRAPH OF THE UTR-2 RADIO TELESCOPE

A. A. Stanislavsky*, A. A. Koval, A. A. Konovalenko and E. P. Abranin

Institute of Radio Astronomy, 4 Chervonopraporna St., 61002 Kharkiv, Ukraine

December 6, 2011

Abstract

The broadband analog-digital heliograph based on the UTR-2 radio telescope is described in detail. This device operates by employing the parallel-series principle when five equi-spaced array pattern beams which scan the given radio source (e.g. solar corona) are simultaneously shaped. As a result, the obtained image presents a frame of 5×8 pixels with the space resolution $25' \times 25'$ at 25 MHz. Each pixel corresponds to the signal from the appropriate pattern beam. The most essential heliograph component is its phase shift module for fast sky scanning by pencil-shape antenna beams. Its design, as well as its switched cable lengths calculation procedure, are presented, too. Each heliogram is formed in the actual heliograph just by using this phase shifter. Every pixel of a signal received from the corresponding antenna pattern beam is the cross-correlation dynamic spectrum (time-frequency-intensity) measured in real time with the digital spectrum processor. This new generation heliograph gives the solar corona images in the frequency range 8-32 MHz with the frequency resolution 4 kHz, time resolution to 1 ms, and dynamic range about 90 dB. The heliographic observations of radio sources and solar corona made in summer of 2010 are demonstrated as examples.

*e-mail: alexstan@ri.kharkov.ua

1 Introduction

Comprehensive information on the physical processes that accompany solar activity can be obtained only with engaging of an extensive scope of observation means. At the meter wavelengths, radio spectrographs, heliographs and polarimeters are widely used to meet this purpose [1]. A worse situation is the case for decameter wavelengths. In particular, the heliograph realization is technically a rather labor intensive problem. Obtaining the high-resolution images (being one of the major demands in application of heliographs) at that low frequencies requires the huge size antennas (> 1 km). At the same time, the heliograph can help obtain new useful information on the extremely multifarious types of bursts being rather specific to this range of frequencies.

Any heliograph has essential advantages in the case it ensures the possibility of simultaneous observations at several frequencies. Multi-frequency measurements of the positions of sources of Type II and III bursts allow to immediately determine the velocity of shock waves and this of electron beams which are propagated in the solar corona. Of substantial interest are the measurements of the velocity of electron beams generating Type III and IIIb bursts at different trajectory phase. The positional measurements at several frequencies will probably permit evaluation of the magnitude of visible displacement of burst sources with respect to their true position caused by the refraction and scattering of radio waves in corona.

Thus, the heliograph permits observation of an angular structure of burst sources and its evolution during their lifetime, as well as to identify the bursts with the appropriate activity regions and measure their heights above the photosphere. The position measurements of double Type IIIb-III, III-III bursts and drifting pairs allow to find out whether the both components are excited in the same place of the corona and at which plasma frequency. Of special interest are the investigations of properties and determination of the positions of coronal mass ejections, frequently

associated with the Type II bursts. This phenomenon is considered a key one in the problems of solar-terrestrial relationships and space weather.

No less interesting direction of the research efforts are observations of the two-dimensional brightness distributions across the quiet Sun at the decameter waves. At the same time, as is known, just at the heights where the decameter radiation is generated there exists the most interesting corona region where the solar wind originates. The here-presented far from exhaustive list of problems capable of solving with the heliograph makes its construction a rather attractive idea. Especially, in case if there is an opportunity of using the available antenna system suitable for this purpose.

To date, there exist not too many radio telescopes permitting to obtain 2D heliograms of the Sun and other sky radiation sources. In the microwave range, they are represented by the Nobeyama heliograph (Japan) operating at two frequencies, 17 and 35 GHz [2], and the RATAN-600 based heliograph (Russia) operating at 3.75 GHz [3]. Roughly within these frequency ranges, the observations are also made at the Siberian Solar Radio Telescope (Russia) [4] at 5.7 GHz, and at the Owens Valley Radio Observatory interferometer (USA) within 1-18 GHz, whose whole range being split into 86 individual subbands [5]. The anticipated Chinese heliograph being designed for radio measurements within 0.4-15 GHz [6] can be considered belonging under the promising instruments, too. For centimeter and meter wavelength radio astronomy investigation, used are the Nancay radioheliograph (France) [7], operating only at frequencies 169, 327 and 408 MHz, and the Gauribidanur radioheliograph (India) which surveys at some individual frequencies within 40-150 MHz range [8]. Since 1969 till 1984, the Culgoora radioheliograph (Australia) [9] was functioning at frequencies 43, 80, 160 and 327 MHz. Note that very few instruments were used at the decameter wavelengths. In this respect we may mention the Clark Lake Teepee-Tee radio telescope (USA) [10] at which the measurements at some individual frequencies within 15-125 MHz were made. Though for

now, it is already put out of service. It will be observed also that developing the antenna arrays capable of operating low frequencies (decameter wavelengths) is connected with heavy technological and methodological difficulties. This frequency range is subject to very heavy noise conditions, the ionosphere exerts an essential impact on the behavior of decameter wave propagation, and achieving the narrow beam pattern requires antennas of huge areas. For instance, the Nancay Decameter Array (Nancay, France) [11] is effectively used for getting dynamic spectra of solar radio emission, while because of its small sizes practically never used for heliographic observations. On account of these reasons, nowadays only a few decameter range antenna systems exist capable of performing heliographic observations, though they also have limited capacities, and thus need upgrading, or even new antenna systems should be built. Suffice it to mention the promising projects LOFAR [12, 13] and LWA [14] which are to be put into service in the near future. Therefore the researches carried out with the UTR-2 based heliograph are of great scientific interest, making up for a deficiency in the knowledge of physical processes on the Sun and/or in the circumsolar space. Note that until now, the UTR-2 radio telescope remains the world-largest and most effective instrument operating within 8-32 MHz, and it is expected to remain that kind performer in long-term future. Accordingly, its intensive design improvement, instrumentation and usage (this including in heliographic mode, too) promises a vast deal of useful astrophysical information.

The high solar activity is frequently accompanied by sporadic radio emission in the meter and decameter wavelength ranges [1, 15]. Some of its types (I, II, III and IV) are common for these ranges. At the same time, they have their inherent specificity. For instance, the Type I bursts, most frequent at meter waves, are practically not observed at the decameter wavelengths. On the other hand, the short-lived stria-bursts, drifting pairs, Type IIIb bursts are met only at frequencies below 60 MHz, though the

latter, along with Type III bursts, are the most numerous events of the solar decameter radiation [16].

The solar decameter sporadic radiation has begun to be systematically studied with the work of Ellis and McCulloch [17]. Since then, a substantial progress was reached in understanding its nature. Meanwhile, the theoretical formulation of the mechanism and conditions of solar burst generation cannot yet give, in most cases, an adequate representation. Therefore further analysis of new experimental data, including those observed with the heliograph, is of current importance.

The present paper is devoted to the UTR-2 heliograph construction, its general functional scheme and discussion of its most important features. In Section 2 we start with the history of heliograph studies in our institute. The basis of any radioheliograph, the UTR-2 based heliograph making no exception, is the antenna system. In Section 3, this latter brief description as applied to the heliograph design, as well as the detailed analysis of the modern configuration of a two-dimensional decameter wavelength heliograph based on the UTR-2 T-shaped antenna system (in Sections 4 and 5), are presented. Next, Section 6 is aimed at design description of the most important UTR-2 based heliograph element, namely the phase shifter for fast beam scanning. The phase shifter essential parts are the switched coaxial delay-line cables. In Section 7 the method is described for calculating the lengths of these switched cables. The heliograph control unit helps to generate the pulse train for switching the fast scanning phase shifter and scan markers generation (see Section 9). Consequently, the UTR-2 array pattern beam is scanning the desired sky area, and the heliograph scan sector format is discussed in Section 8. Further, in Section 10 we consider the operation features of the heliograph receiver-recorder. It is based on a multichannel digital spectropolarimeter (DSP). In Section 11 we present the preliminary results of test observations made with the considered instrument in summer of 2010. In conclusions, we summarize the heliograph

development and prospects for its future application in radio astronomy observations at decameter wavelengths.

2 Brief History of Heliograph Studies in the UTR-2 Observatory

The first positional observations of solar radiation with the use of a two-dimensional heliograph based on the UTR-2 radio telescope were made during July 31 to August 11, 1976 [18]. At that time, the enhanced radiation was associated with emerging of the active McMath No. 14352 region on the eastern limb which, while moving westwards, was intersecting the entire solar disk. For the aforesaid period of observations, numerous Type III and IIIb bursts, Type IIIb-III bursts, as well as short-lived narrow-band stria-bursts being components of the Type IIIb burst chains were recorded. The daily two-hour measurements centered for the local mid-day were made at the operating frequency 25 MHz, and also in parallel by the "North-South" (N-S) antenna array to which output the dynamic spectrograph for the 23.5-25.5 MHz band was mounted. The recorded heliograms permitted constructing the histograms of coordinate distribution of effective centers of Type III and stria-bursts for hour angle (h) and declination (δ) in the selected days for different positions of solar disk active regions. The positional data on the average coordinates of burst sources centers were used to obtain the day-to-day dependence of the radiating region position. The motion velocity of the active region, crossing the solar disk westwards, permitted estimates of the average heights R_s (being radial distances from the Sun's center) of the Type III burst and stria-burst sources during the radio burst. The heights R_s were determined by several methods which yielded close results. In the meter and centimeter wavelengths, the radial distances of the coronal emitting regions were calculated in papers [19, 20]. The R_s values estimated with the UTR-2 heliographic

observations have appeared comparable to each other and corresponded to those first obtained at decameters during the interference measurements at the Clark Lake Radio Observatory (CA, USA) at 30 MHz while investigating a number of solar noise storms [21]. The heliograms have permitted the conclusion that the stria-bursts of IIIb chains and Type III bursts appear about the same place on the Sun's image plane.

Further research efforts, assisted by the UTR-2 antenna system operating the mode of a two-dimensional heliograph, were largely concentrated on studying the Type IIId radiobursts with echo components [22, 23, 24, 25, 26, 27, 28]. The decameter Type IIId bursts were first recorded at the UTR-2 observations of July 6, 1973. Narrow-band elements of this emission fine structure – the diffuse stria-bursts – are a variety of ordinary short-lived stria-bursts, of which the dynamic spectra of Type IIIb bursts are patterned. The principal feature of diffuse stria-bursts consists in that their form largely depends on heliolongitude of the coronal sources region. When the Type IIId source is in the near-limb region, the stria-bursts with steep fronts and sharp peaks are observed monotonically damping in a few seconds. With the active region approach to the central solar meridian, the time splitting occurs, i.e. the echo-like component of bursts with growing delay appears. The echo-burst delay time becomes maximum when the emitting region traverses the central meridian. The appearance of an extra burst echo-component and the delay variation with heliolongitude are qualitatively explained by using a simple model of a point pulsed source placed into a spherically symmetric corona and emitting at the plasma frequency second harmonic [29]. Using this kind model in interpreting the origin of Type IIId bursts was suggested in papers [22, 23]. However, the theoretically calculated values were poorly coordinated with those UTR-2 measured. The assumption [28] was therefore made that the echo-component of stria-bursts is formed not merely due to the reflection from a deeper layer of a spherically symmet-

ric corona, but also as a result of the refraction of radio waves on some large-scale coronal structures. This hypothesis has been supported in [30] where the author has mathematically simulated the shaping of Type IIId bursts. During the systematic researches of the Sun with the UTR-2 array system and positional observations with the two-dimensional heliograph for almost two decades, more than 10 solar Type IIId burst storms were recorded. It will be observed that Type IIId radio bursts are rather rare events, unlike Type III bursts being most mass events of the decameter sporadic solar radiation. With the complex observations using the two-dimensional heliograph, in June 1984 during a week-long Type III storm, about 1000 bursts were recorded at 25 MHz. The data obtained allowed the statistical sample manipulation of decameter events by employing the cluster analysis [31]. For the statistical procedure of sample ordering and clustering, used were such parameters of bursts as time delay between the two sequent bursts, burst duration at half-power level, maximum intensity and degree of circular polarization.

It should be recalled that way back in the mid-nineties, the radioastronomy observations with the UTR-2 array were made only near to several fixed frequencies: 10.0, 12.5, 14.7, 16.7, 20.0 and 24.8 MHz, while the broadbandness of this antenna system is much greater. On the other hand, in the capacity of a recorder, e.g. for the heliograph, the FTAP-2 facsimile set was used recording the signal on a electrochemical paper with the dynamic range making only 10-16 dB. Such a situation urgently demanded extensive design improvement of the whole UTR-2 hardware facility. When the UTR-2 antenna amplifier system had been upgraded in the late nineties, the measurements became possible in the continuous frequency band of 10-30 MHz and more [32]. Thereupon, an exigency of installation of appropriate recording equipment arose. With that end in view, for multi-frequency observations a 60-channel spectrum analyzer was put into service which included 60 separate frequency-tunable within 10-

30 MHz radio receivers with the 4-10 kHz bandwidth. The next step was applications of digital multichannel (1000 and more channels) spectrum analyzers (digital receivers). These latter already allowed covering the entire UTR-2 array frequency range with the frequency separation of about 4 kHz, as well as recording on digital storage media and perform varied signal computer processing [33, 34, 35].

The very first configuration of the UTR-2 array based heliograph was as follows. By means of a special beam control system of the UTR-2 array it became possible to quickly scan the sky area under investigation. Its image was recorded through signal injection from the outputs of N-S and E-W ("East-West") antennas into the sum-difference device. The sum and difference signals were amplified by individual receivers with square-law detectors. The outputs of square-law detectors were in opposition, thus providing the difference of their output voltages. This difference voltage then fed the final recorder input. Actually, the radio astronomy research efforts are basically carried out using the digital receiver-recorder, being a digital spectropolarimeter (DSP) capable of signal receiving and processing, and data recording on the PC hard disk. Surprisingly, we still face the fact that though the UTR-2 based heliograph was designed long ago and used in diverse radioastronomy researches, its complete and thorough description had been postponed because of ever-lasting upgrading its hardware environment. For this long period, the heliograph has been essentially reengineered, new possibilities for its application appeared, and things have reached an exigent necessity point to describe the heliograph development at long last review.

3 Antenna System

Using the available antenna system for the heliograph appliance has in many respects determined its circuit design. The UTR-2 radio telescope

operating within 10-30 MHz has been described in detail in papers [36, 37]. Here in this paper, we will only touch some of its array antenna features being all-important of understanding the operation of the heliograph as a whole.

The UTR-2 array antenna system consists of three rectangular array arms: northern, southern and western. Each of the first two array arms (N and S) includes 120 rows (each possessing 6 fat, therefore broadband, horizontal dipoles) lined along the parallel. The E-W array has 6 rows (each possessing 100 fat horizontal dipoles) lined along the parallel (see Fig. 1). The horizontal dipoles of all arrays are oriented along the east-west line. Along the parallel, they are spaced by 9 m, and 7.5 m along the meridian.

In the arrays with staged (otherwise stepped or storied) layout, the signals of horizontal dipoles are summed and phased with discrete cable delay lines. The signals are phased independently by the two systems in two orthogonal coordinates, V and U, which are connected to equatorial coordinates with the relations

$$U = \cos\delta\,\sin t\,, \quad V = \sin\beta\cos\delta\cos t\ - \cos\beta\sin\delta\,, \tag{1}$$

where t and δ are an hour angle and declination, respectively, and β is the geographic latitude of antenna location.

The E-W antenna has one-stage phasing in V-coordinate and three-stage phasing in U-coordinate, while the N-S antenna one-stage phasing in U-coordinate and four-stage phasing in V-coordinate. The circuit design allows signals' summation and phasing in a manner that each array before the last phasing stage appears to consist of four sections. But for all that, each section has no common circuit elements with the others and combines 1/4 of horizontal dipoles of the corresponding array. To provide the best received signal-to-noise ratio, the signals from all sections are amplified by array-distributed individual amplifiers.

Figure 1: East-West arm of the UTR-2 radio telescope.

The amplified signals of eight sections of the N and S arrays are phased, amplified by a line of antenna amplifiers, then each of the signals furcating with the hybrid splitters into 5 channels. The N-S antenna 5 beams, distributed in the V-coordinate at $\Delta V = 1/150$, are shaped by phasing with the constant delay of each of the channels of all eight sections and further summation. In this case, the third beam is summed in phase, thus shaping the central beam toward phasing (U, V_3). Beam directions along the V-coordinate are determined through the relation

$$V_n = V_3 - \frac{n-3}{150}\,, \tag{2}$$

where n is the number of a beam counted from the southward direction. The directions of all 5 beams lie in one plane V, for which $U_0 = \text{const}$ and their hour angles, following the relation (1), are equal

$$t_n = \arcsin(U/\cos\delta_n)\,. \tag{3}$$

Since in beam phasing, the time delays used are constant, the declination distance between beams will be

$$\Delta\delta \approx \Delta V/(\cos\beta\cos\delta + \sin\beta\sin\delta\cos t)\,, \tag{4}$$

where t and δ are an hour angle and declination of antenna phasing direction (in the zenith direction $\beta = \delta, t = 0$ and $\Delta\delta = 23'$).

For shaping pencil beams, each E-W antenna output is multiplied by one of the N-S antenna five beams. In this case, at 25 MHz, the zenithal beams have sizes $28' \times 27'(t \times \delta)$ at half-power width. As to the receiving of side-lobe radiation, it is known to appear larger within the angles of factors of the narrow sides of arrays in the mode of multiplication of the T-shaped aperture arms. Its maximum power at the equi-amplitude distribution of antenna currents makes about 22%, i.e. the same level as that for the field array pattern. The side-lobe received radiation contribution is controlled by varying the amplitudes of the N-S antenna section currents.

The antenna has several types of phase shifters – those with different number of inputs and increments, as well as those with summation of signals after and without phasing. The signal from each input of the phase shifter comes upon a series of switched binary-incremental cable time-delay lines. In essence, the series are the separate phase shifters structurally making one shifter. As switching elements, the high-frequency electromagnetic relays are used with the pickup time of ~ 20 ms and cyclic life of $\sim 10^5$ switchings. The phase shifters are remotely controlled from the control panel either manually or using the PC user-defined program.

The telescope coverage area is limited to $-1 \leq V_0 \leq 1$ and $-7.5/9 \leq U_0 \leq 7.5/9$. In these limits, the directional pattern of all stages of the both independent systems of array phasing can be varied. The antenna employs asynchronously steered patterns of array stages, i.e. their directions may differ. In this case, the number of increments (and thus their values) of phase shifters of array stages is selected reasoning from the allowable decrease of directivity of antennas shaping the corresponding directional patterns. Since with approaching the array output the beam width of horizontal dipoles phased by one phase shifter of a stage decreases, the number of increments in the stage increases. The maximum number of increments has only phase shifters of the last stages where the sections of E-W and N-S antennas are phased. The E-W antenna has the phase shifter for 4 inputs and 10 bits, i.e. possessing the $2^{10} = 1024$ number of increments over U; the N-S antenna having the phase shifter for 8 inputs and 11 bits providing $2^{11} = 2048$ beam positions over V within the whole coverage sector.

The beams over U and V are convenient to number as $0 \leq |N_U| \leq 511$ and $0 \leq |N_V| \leq 1023$, attaching to them a negative sign if the beam is directed accordingly eastwards and northwards (similarly to the U and V coordinates). Making allowance for the sign or quadrant choosing is performed by the high-order digits of phase shifters, while the rest 10 bits

over V and 9 bits over U are intended for recording of the absolute values of beam numbers. The beam numbers over U and V are related to the phasing direction (U, V) as

$$N_U = 512\frac{7.5}{9}U - 0.5\ \mathrm{sign}(U), N_V = 1024V - 0.5\ \mathrm{sign}(V)\,. \qquad (5)$$

Here, the function $\mathrm{sign}(x) = \begin{cases} 1, \text{ if } x > 0; \\ -1, \text{ if } x < 0. \end{cases}$

To optimize the magnitude of phase errors due to asynchronous beam control, the phase shifters are designed so that the array beam cannot be directed precisely to zenith. In the initial position, the switching delays are switched off in all phase shifters. However, due to the use in phase shifters of permanently engaged time delays, the directions of patterns of array stages appear to be displaced by the 1/2 of the corresponding stage increment.

Since in the general case the array beam direction is determined by the product of directional patterns of stages possessing noncoincident directions, the antenna beam phasing direction does not, strictly speaking, coincide with either of UTR-2 antenna factors. However, with taking into account that in both coordinates the antenna beamwidth is more than 8-fold narrower than the section directivity diagram, the phasing direction will most closely coincide with the direction of the sharpest factor. As the computing shows, the error in this case will not exceed $0.6'$ over t and $0.4'$ over δ, which can be neglected.

In that case, within the coverage sector, the radio telescope beam can be positioned to any point of the sky accurate to no worse than 1/2 of the magnitude of the sharp UTR-2 antenna factor increment. In the equatorial coordinates, the error in beam pointing, due to the control increment, will depend upon beam direction. Within the angle sector where the solar observations are made, it reaches a well noticeable magnitude (approximately $3.5'$ and $2.5'$ over t and δ, respectively). The account for a phasing increment of the antenna sharp factor is therefore desirable.

To determine the true direction of the radio telescope (third) beam phasing (U_0, V_3), it is sufficient – with the given calculated phasing direction (U, V) and using formula (5) – to find the corresponding magnitudes of N_U and N_V. We may round off them to the integral value using the formula

$$N^* = \text{int}(\text{abs}(N)) \cdot \text{sign}(N)\,, \tag{6}$$

where $\text{abs}(x)$ is the absolute value of x, and $\text{int}(x)$ is its integer part. Just these numbers of beams (N_U^*, N_V^*) correspond to the true phasing direction which is found using the relations from (5), namely

$$\begin{aligned} U_0 &= (\text{abs}(N_U^*) + 0.5)/614.4 \cdot \text{sign}(N_U^* + 0.5), \\ V_3 &= (\text{abs}(N_V^*) + 0.5)/1024 \cdot \text{sign}(N_V^* + 0.5)\,. \end{aligned} \tag{7}$$

In case of necessity, the direction of beams (U_0, V_n) in the equatorial coordinates can easily be found with the aforementioned relations.

4 Scanning System

The UTR-2 scan sector allows one to observe the Sun for about $\pm 4^h$ around local noontime. Practically, however, due to ionospheric screening at large zenith observation angles, growing number of interfering broadcasting radiostations, and the heliograph space resolution decrease, the scan sector is limited over declination, $\delta_\odot \geq 10^\circ$, and over hour angle, $|t_\odot| \leq 30^\circ$.

The five-beam UTR-2 operation and beam control in the two, U and V coordinates, allows in principle to use this array without any reconstruction as a 2D heliograph with either serial or parallel-serial scan. Moreover, by having formed several beams of the E-W arm in the U coordinate, a parallel scan heliograph can be built in which the maximum sensitivity is possible. However, no advantage is taken of the opportunity so far seeing that a sufficiently great amount of newly fabricated equipment is needed in this case.

To observe both disturbed and quiet solar radio emission (for which purpose the standard recording equipment of the radio telescope is used) the parallel-serial scan system can be applied. In this case, the output signals of all five beams of the N-S and E-W antennas are simultaneously recorded by five parallel receiver channels. As for the solar radio emission observations with the heliograph employing the series principle, only one receiver-recorder set is required as distinct from the previous case.

In the both cases, the five-beam set located in the V plane sequentially holds a number of positions over U. It is achieved by the E-W array pattern scanning. Since the beams are of about the same size both in the U and V coordinates, obviously it is expedient to take equal distances between them in these directions, i.e. $\Delta U = \Delta V = 1/150$.

The gain in outlay for recording equipment – in the case of using the sequential as against the parallel-serial scan – is particularly appreciable in view of decisive expediency of heliograph operation simultaneously at different frequencies. Certainly, with lower frequencies, the observation efficiency worsens because of the low space resolution. Even at 25 MHz, this latter appears insufficient for the rather important measurements of brightness distribution of solar decameter radiation sources. However we must bear with this keeping in mind that in this case we are dealing with the decameter wavelength range. Realization of antenna systems for this range, whose sizes would be much greater than these of the UTR-2 array, is rather problematic in itself. Besides, the antenna size restriction takes place at decameter wavelengths due to the ionosphere induced decorrelation of the received signal.

5 Heliograph Functional Scheme

With the above mentioned requirements taken into consideration, the heliograph functional scheme was suggested and is shown in Fig. 2. The

heliograph system incorporates the E-W and N-S antenna arrays, too. An extra phase shifter (for fast scanning) is sequentially connected to the E-W antenna section outputs. The beam shaper phases and sums up the antenna section signals, and then, using the splitters, it shapes a five-beam directional pattern. The N-S and E-W beam arm switches connect in turn the signals of a five-beam set, and also the noise signal from the marker shaper to the DSP. The marker shaper is integrated into the noise generator and generates the right ascension separating markers as well as markers of end (beginning) of image on heliograms. The signal strength of the marker of end (beginning) of image is higher than the separating marker between the five-beams due to the incorporated 3 dB attenuator. This permits avoiding difficulties in analyzing the heliograms. The control unit ensures the beam switching, markers shaping and phase shifting of fast scanning.

In what follows, we will dwell on some important features of the considered device.

5.1 Heliogram Repetition Rate

The heliograph image repetition rate should be rather high so that the burst evolution could be observable. However, a too high repetition rate will reduce the receiver sensitivity and complicate the recorder design. The maximum image repetition rate was taken 4 fps. At such a repetition rate, the heliograph allows observation of the bursts with duration of ≥ 1 s that is quite sufficient for the given range of radio observations. In this case, the receiver sensitivity remains high enough, while the recorder simple and compact. That high frequency of a heliograph image repetition rate is not always required. It can be lower as well (e.g. for observations of the quiet Sun radio emission). Such a possibility is provided by the change of clock rate in the control unit.

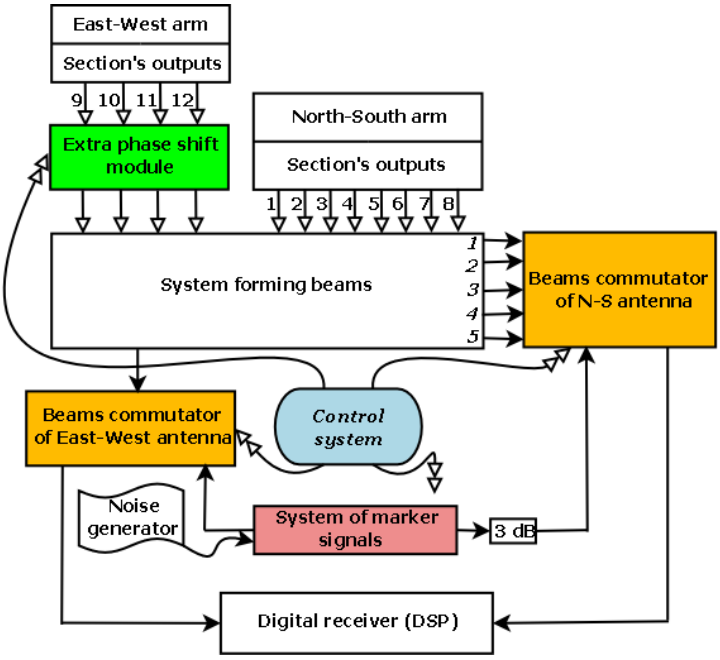

Figure 2: The heliograph block diagram sketch.

5.2 Polarization and Frequency Passband

While observing the sporadic radio emission of the Sun, in addition to the bursts' position measurement, determining their polarization is of great interest, too. However because of the fact that the UTR-2 array antennas are designed to receive only the linear polarization, the polarization measurements are impossible.

For the better signal-to-noise ratio, the frequency passband should be wide enough. The upper limit of the passband width is determined by the frequency band of the observed phenomenon ($\sim$ 1 MHz). On the other hand, the noise density and intensity from the short-wave broadcasting stations are extremely great at the decameter wavelengths. For this reason, the passband width cannot be greater than several kilocycles. Therefore the entire recording band of 10-30 MHz can be conveniently subdivided by the channels of $\sim$ 4 kHz. As will be shown below, the DSP perfectly copes with such a task.

5.3 Switches

In a heliograph with sequential shaping and recording of image elements, the receiver-recorder is sequentially connected to the outputs of the N-S antenna five beams. In the end of each beam scanning cycle, instead of antennas, the auxiliary noise generator – which helps forming markers on the heliogram – is connected to the receiver-recorder.

The heliograph incorporates two switches: the N-S antenna beam switch and the E-W antenna switch. The former is used for the sequential connection of the outputs of the N-S antenna five beams and the auxiliary noise generator to one of the receiver-recorder inputs. The E-W antenna switch connects to the second input of the receiver-recorder either the E-W antenna output, or the auxiliary noise generator. The E-W antenna remains connected to the receiver-recorder for the whole beam scanning period. In

the end of each scanning cycle of the kind, the auxiliary noise generator is connected, instead of antennas, to the both inputs of the receiver-recorder.

Thus, the E-W antenna switch has two inputs and one output (the first input is fed by the E-W antenna output signal, while the second by the signal for forming a marker of the end of scanning five beams). The N-S antenna beams switch has six inputs and one output (five inputs for connection of outputs of N-S antenna five beams, while the sixth input is fed by the signal forming a marker of the end of scanning beams and transfer to the next scanning cycle). While the E-W antenna pattern rests in the predetermined position, several cycles of scanning N-S beams can be performed. The signal from the first input of the E-W antenna switch feeds the switch output for the time of scanning five-beam set of the N-S antenna by its switch. The second input signal feeds the output when the sixth input beam switch is switched on. Thereby, in this case the signals from the N-S and E-W antennas outputs are disconnected from the inputs of the receiver-recorder, and instead the signals for forming a marker, which indicates the end of scanning five beams, are connected.

Concurrently with the eighth marker of end of scanning five-beam set, the end-of-image marker should be shaped to avoid possible errors in determining the frame boundary in time. The end-of-image marker can be combined with the time marker provided the UTR-2 array's code-switch time is matched with the E-W array pattern switching time.

The E-W antenna arm switch consists of two, while that of the N-S arms of six identical cells in which the crystal fast-response and long-lifetime diodes are used as switching elements. For removal of reflections from the unloaded inputs of disconnected channels, all of them are loaded by the matched loads of 75Ω for a disconnection period. The attenuation in open channels of switches makes $\sim$ 1.2-1.5 dB and is largely determined by losses in switching diodes. Structurally, the N-S and E-W antenna beam switches are made as the two separate printed-circuit boards. Each switch has a

monitoring circuit that allows fast detection of malfunctions to appear in operation.

6 Fast Scan Phase Shifter Design

The heliograph beam control system has two functions: a rather slow Sun tracking and fast scanning over the heliograph scan area.

Though the UTR-2 radio telescope was designed as a multi-functional instrument, its phasing system does not allow long observations with fast beam scanning because of electromagnetic relays used in it. That is why the heliograph utilizes only the UTR-2 phasing system for tracking the Sun with the beam switching rate of several minutes. As for the fast scanning, this function is executed by a specially designed phasing system.

This latter, as has already been noted, should discretely change the E-W array pattern position over U. The complexity of the beam fast scan system is determined by the point of its connection to the UTR-2 antenna phasing circuit seeing that it should embrace all the subsequent stages and never do any of the previous ones. From the point of simplicity, it is expedient to be connected as near as possible to the array output.

On the other hand, the point of its connection is determined by the heliograph scan sector in the U coordinate. Its width should be comparable to (or less than) the one of the antenna beam patterns of the elements which are phased by this stage. On the last stage, where the E-W arm section output signals are phased, the field beamwidth makes about $\sim 3^\circ$ at 25 MHz. Such a scan heliograph sector over U appears to be quite sufficient even for observation at 12 MHz, where the solar corona radio diameter makes about 1.5°. For switching on the fast scan system at the last phasing stage, only one 4-input phase shifter is required.

The beam fast scan phase shifter is circuit-connected between the section outputs and corresponding inputs of the last E-W arm phasing stage. In

this case, the section beam pattern appears to be a scanning beam envelope.

Structurally, the fast scan phase shifter is similar to that used in the UTR-2 phasing system [38]. The difference lies only in that its coaxial cable lengths are switched with the diode keys which have larger service life and operating speed ($\sim$ 0.5 ms). The phase shifter integrates four lines, each being a three-digit digital-binary time delay line. For short, we hereinafter will use the abbreviation of this phase shifter as the type FV4-3 (ФВ4-3 in Russian transcription). Among themselves these strips differ only by the values of switched time delays. The control circuit for the isobits of all strips is connected in parallel.

Using the diode keys and the coaxial cable lengths as the time delays ensures broadbandness for such a phase shifter. The signal phase deviation from the calculated value does not exceed 5° at 25 MHz. The initial cable lengths in the phase shifter strips (ℓ_0) are selected so that in the starting position (when all delays are switched off) the E-W arm beam appears to be located eastwards to the U_0 phasing direction. As the phase shifter passes through all its 8 positions, the beam with a step of $\Delta U = 1/150$ moves westwards.

It is natural to take the scan sector being located symmetrically with respect to the U_0 phasing direction. As the number of phase shifter positions is even, neither of its positions does coincide with the U_0. The five-beam set scanning over V sequentially takes the values over U, so that

$$U_m = U_0 + \frac{m - 4.5}{150}\,, \tag{8}$$

where the beam position number $1 \leq m \leq 8$. In this case, no N-S antenna phasing over U is required as its pattern width is greater versus the E-W antenna scan sector. Only the cable length to compensate the average electrical length of the fast scan phase shifter is additionally connected to the N-S antenna.

To calibrate the heliograph receiver-recorder chain, the electrical lengths

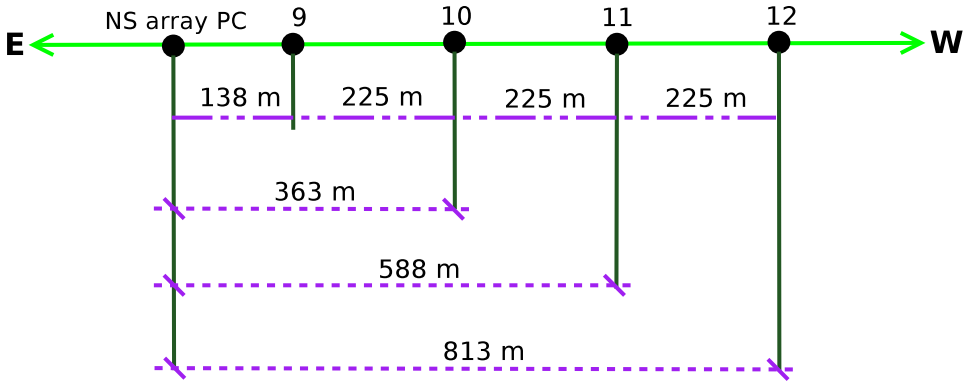

Figure 3: Spatial position of the N-S array phase centers (PC) and E-W arm sections (figures 9, 10, 11, and 12 denote section numbers).

of the E-W and N-S antennas should be equalized. As for $U_0 = V_0$ and for any m, according to expression (8) we have $U_m \neq 0$, the additional cable delays should be used for compensation. In operation mode they are switched off.

7 Calculation of Cable Lengths for FV4-3

In heliograph operation, the maximum additional UTR-2 beam deflection over U, with respect to the direction given by the array phasing system, makes $\Delta U = \pm 7/300$. The phase center of the heliograph fast scan phase shifter FV4-3 is combined with the N-S array phase center (being a phase shifter with the displaced phase center). Fig. 3 shows the spatial position of N-S array phase centers and E-W arm sections.

To equalize the phases of received signals at the outputs of all antenna system elements, the natural path differences L, l_1, l_2, l_3, and l_4 are compensated with additional delay line lengths (cables) connected in the FV4-3 (see Fig. 4). The electrical lengths of additional delay lines have the values L_z, l_{z1}, l_{z2}, l_{z3}, l_{z4}, and in this case $L_z = l_4$, $l_{z1} = L - l_1$, $l_{z2} = L - l_2$,

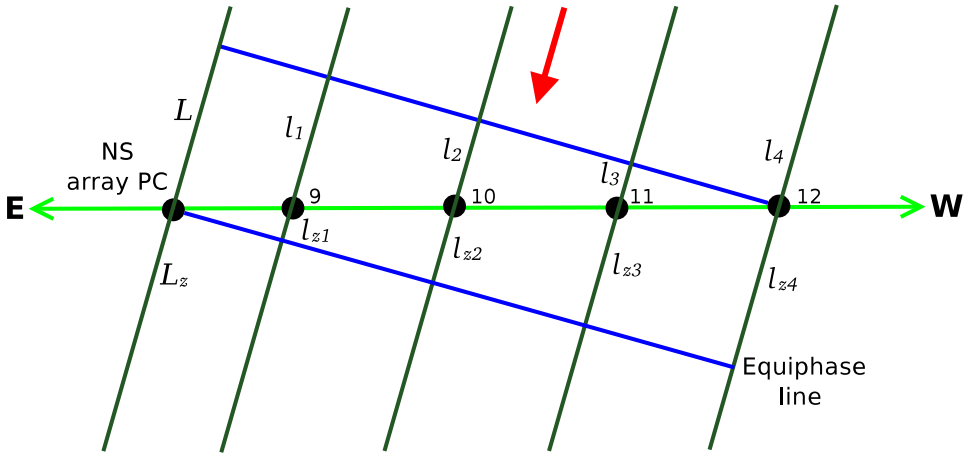

Figure 4: Compensation of path differences by connecting some additional delay-line lengths (L_z, l_{z1}, l_{z2}, l_{z3}, l_{z4}).

$l_{z3} = L - l_3$, $l_{z4} = L$.

For the beam eastward deflection and for the unchanged phase center position in the N-S array center, the path differences should be compensated by connection of negative lengths in the E-W array, which is impossible. Therefore the phase center is displaced by connection of the additional length $L_z = l_4$ (Fig. 5). This additional length remains permanently connected with the beam deflection both eastwards and westwards, while the compensating lengths in the FV4-3 change respectively.

As the maximum heliograph beam deflection over U is $\Delta U_{max} = \cos\alpha = 7/300$ and the maximum distance between the extreme phased elements $L_m = 138 + 3 \cdot 225 = 813$ m, then $L_z = L_m \cdot \cos\alpha = 813 \cdot 3/700 = 18.97$ m. For the eastward deflection, the phasing electrical lengths are as follows

$$\begin{aligned} L_0 &= L_z\,, \\ l_{01} &= 225 \cdot 3 \cdot 7/300 = 15.75 \text{ m}\,, \\ l_{02} &= 225 \cdot 2 \cdot 7/300 = 10.5 \text{ m}\,, \\ l_{03} &= 225 \cdot 7/300 = 5.25 \text{ m}\,, \\ l_{04} &= 0. \end{aligned}$$

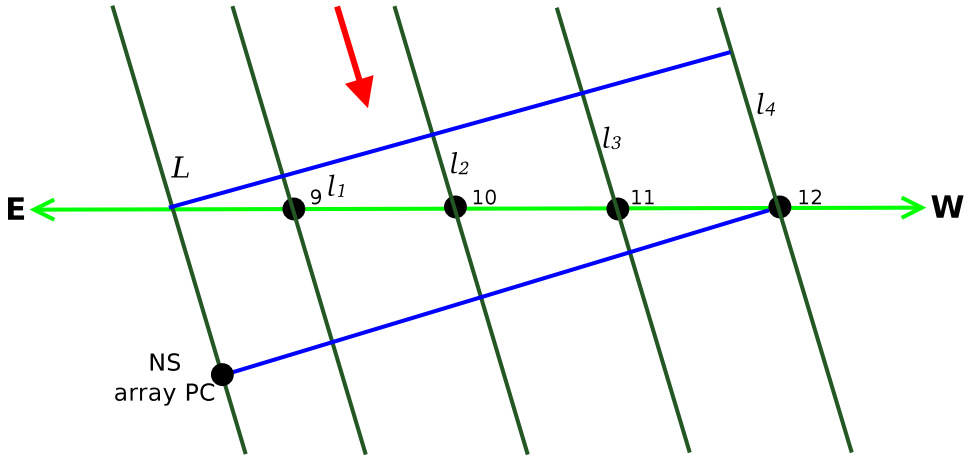

Figure 5: N-S array phase center (PC) position displacement by connecting some permanent length L_z for the beam deflection eastwards.

For the westward deflection, the phasing electrical lengths make

$$\begin{aligned}
L_z &= 0 + l_{z4} = 0 + 813 \cdot 7/300 = 18.97 \text{ m}\,, \\
l_{z1} &= 138 \cdot 7/300 + L_z = 3.22 + 18.97 = 22.19 \text{ m}\,, \\
l_{z2} &= (138 + 225) \cdot 7/300 + L_z = 8.47 + 18.97 = 27.44 \text{ m}\,, \\
l_{z3} &= (138 + 2 \cdot 225) \cdot 7/300 + L_z = 13.72 + 18.97 = 32.69 \text{ m}\,, \\
l_{z4} &= (138 + 3 \cdot 225) \cdot 7/300 + L_z = 18.97 + 18.97 = 37.94 \text{ m}\,.
\end{aligned}$$

Then, the lengths which are switched in the FV4-3 operation should respectively have the values

$$\begin{aligned}
L_k &= L_z - L_0 = L_z - L_z = 0\,, \\
l_{k1} &= l_{z1} - l_{01} = 22.19 - 15.75 = 6.44 \text{ m}\,, \\
l_{k2} &= l_{z2} - l_{02} = 27.44 - 10.5 = 16.94 \text{ m}\,, \\
l_{k3} &= l_{z3} - l_{03} = 32.69 - 5.25 = 27.44 \text{ m}\,, \\
l_{k4} &= l_{z4} - l_{04} = 37.94 - 0 = 37.94 \text{ m}\,.
\end{aligned}$$

The delay lines are made by employing the binary principle, each having

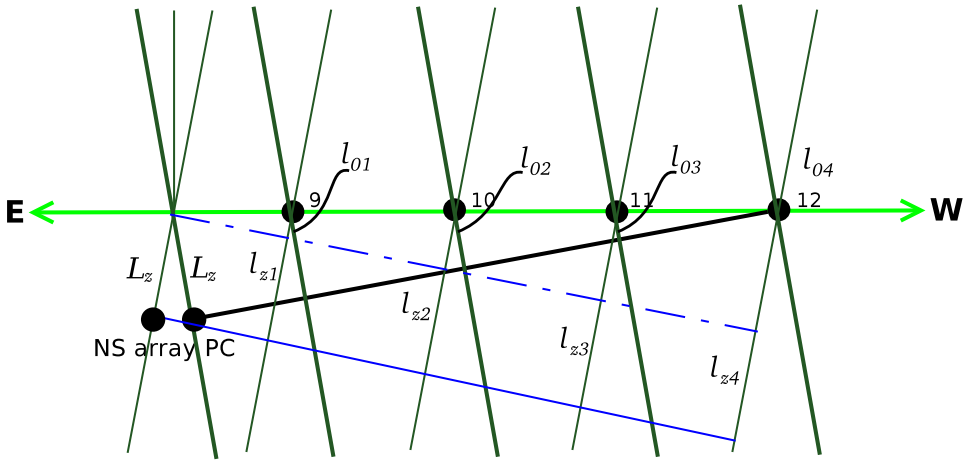

Figure 6: Schematic representation of the UTR-2 array pattern position for the extreme western and eastern positions: L_z, l_{01}, l_{02}, l_{03}, and l_{04} are phasing lengths for the beam deflection toward east; L_z, l_{z1}, l_{z2}, l_{z3}, and l_{z4} are phasing lengths for the beam deflection toward west with allowance for a permanently connected length L_z.

three switched bits. The delay values in the bits are interrelated as 1 : 2 : 4. Besides the switched elements, the delay lines include also the non-switchable elements l_{01}, l_{02}, l_{03} and l_{04}. Such a structure of delay lines allows to discretely set the heliograph beam into eight positions in the U coordinate with a step 1/150 within $-7/300$ to $+7/300$ (Fig. 6). All line bits are switched synchronously.

With the selected structure of delay lines, the length of the least-significant bit $l_{\rm I} = l_k/7$ while that of the second bit $l_{\rm II} = 2\,l_k/7$, and that of the third bit $l_{\rm III} = 4\,l_k/7$. The permanent length connected in the N-S array is equal to $L_0 = 18.97$ m. All the FV4-3 elements are made of the RK 75-9-12 (PK 75-9-12 in Russian transcription) type coaxial cable having the characteristic impedance of 75 Ω and wave shortening coefficient of $k = 1{,}51$. Thereto, for the FV4-3 connection into the UTR-2 phasing system, each delay line should additionally possess two special cables with total length of $l_t = 5$ m. The total length of special cables in each line is added to the length of a non-switchable cable length l_0. The Table 1 shows

Table 1: Phase shifter cable delay line lengths (in meters), l_0 is the initial length, $l_{\rm I}, l_{\rm II}$, and $l_{\rm III}$ are switched lengths.

Length, m	E-W array arm section			
	♯9	♯10	♯11	♯12
l_0	10.43	6.95	3.48	0
$l_{\rm I}$	0.61	1.60	2.60	3.59
$l_{\rm II}$	1.22	3.20	5.19	7.18
$l_{\rm III}$	2.44	6.41	10.38	14.36

the corrected FV4-3 cable lengths with allowance for the wave shortening coefficient and some processing aids into non-switchable delay lines. The special cable length is added also to the N-S antenna cable, thus $L_0 = 17.56$ m.

The phase shifter attenuation with the delay line length variation from 0 to 38 meters changes within 3.3 to 4 dB and is mainly caused by the losses in switching diodes.

8 The Heliograph Scan Sector Format

So, any heliogram is formed owing to the fact that with the fast scan phase shifter, the five pencil beams spaced in the V coordinate take sequential positions in the U coordinate. Thus, the full heliogram of the heliograph scan region is a rectangular matrix of 5 rows and 8 columns (making totally 40 elements) spaced over hour angle and declination by $25'$ (see Fig. 7). The image angular size over hour angle makes $\sim 3.3^\circ$ at 25 MHz.

Such an element number ratio over declination and right ascension allows for the fact that in the close-to-solar-minimum years the equatorial diameter of the solar corona decameter radioimage is almost 1.5-fold exceeding the polar one. Besides, the decameter solar emission sources, as is known, are also crowded in the solar equatorial plane. At the same time,

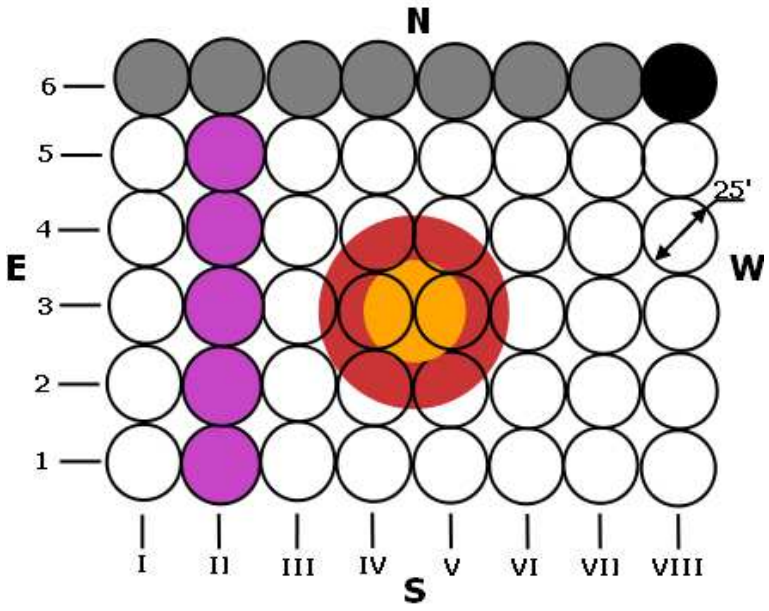

Figure 7: A heliogram field formed by the heliograph with the resolution of 5×8 pixels. Angular size of each element in the t and δ coordinates makes $25'$. Grey and black circles are separating markers.

a whole series of the problems does not require that large scan sector over U. Therefore the possibility for changing the number of elements in lines is provided, thus allowing to increase the frame rate.

In the U and V coordinates, the image elements form a rectangular frame. However the observed data are more preferable to be represented in equatorial coordinates. And from the viewpoint of their obviousness it would be better that the beam antenna pointing to solar disk remained unchanged. Though, as was already noted, in the mode of heliograph Sun's tracking the distances between the beams change both over t and δ. To avoid some extra distortions related to fast scanning over U, the third beam declination should remain constant for all five-beam set positions over U. This can be ensured at each U-step by appropriate N-S array phasing over V. For each U_m, the V value should be such that the right-hand side of expression

$$\sin\delta_{m3} = -V\cos\beta + \sin\beta\sqrt{1-U_m^2-V_3^2} \tag{9}$$

should be constant. Here β is the UTR-2 array geographic latitude.

In order to cope with the above task, an 8-input three-bit phase shifter, as well as more sophisticated phase shifter control equipment, are required. Therefore the heliograph is scanning the five-beam sets only by the E-W arm pattern steering over U.

The UTR-2 array solar tracking system is carried out by superimposition of the scan area center with the solar disk center. Note that the rectangular raster is preserved only for near-meridian operation. In the other cases, the raster shape may essentially differ from the rectangular one. This phenomenon is caused by the fact that in antenna pattern steering, the U or V coordinate changes at fixed values of the other coordinate, while the increment of coordinates ΔU and ΔV are taken constant and independent on the U or V coordinate values. This raster shape feature should be taken into consideration in the observed data reduction, otherwise noticeable errors may result in determination of coordinates of bursts in heliograms.

In overwhelming majority of cases, the burst source center position with respect to the imaging array (Fig. 7) is such that the burst response occupies several image elements. Each element of brightness is determined by its spacing from the burst source center. In data processing, while determining the burst coordinates, the image elements intensity ratios are measured and compared with the imaging array. The imaging array coordinates are calculated beforehand. Such a technique allows determination of the burst angular coordinates to an accuracy of $\sim 5'$.

9 Control System

The operation of fast scanning phase shifters, switches, marker schemes and attenuators is accomplished by the control unit in which the appropriate control pulse sequences are formed.

With the "Reset" command to the control circuit of the FV4-3 phase shifter (being a four-channel switch of binary-discrete three-bit time delay cable lines which are sequentially connected to the four outputs of the E-W array sections), the E-W array pattern is hopping to the extreme "eastern" position (position I, code 000). For this purpose, all the FV4-3 cable delays are disconnected (operating in minimum-delay mode). During heliograph operation, the E-W arm pattern position can discretely change moving westwards (totally 8 positions). In the extreme "western" position (position VIII, code 111), the time delay cable lengths are maximal.

The FV4-3 unit has four switchboards. Their circuits are identical, only the lengths of switched cables are different. The control pulses are sent simultaneously to all four switchboards on the analogous contacts. To connect the required delay line (ℓ, 2ℓ or 4ℓ), the cutoff voltage drop should be applied to the appropriate contacts thus locking the switching diodes connected in parallel to the delay cable, and simultaneously the zero voltage drop be applied to the conjugate contacts to unlock the switching diodes

connected in series to the delay cable. For the delay cable disconnection, the switching voltage should be applied to the appropriate control inputs in the reverse order. In this case, the diodes connected in parallel to the delay cables are on, while those connected in series to the delay cable are off.

For the maximum frame repetition rate (to 4 fps) and number of image elements (48 elements per frame), the clock rate which controls operation of switches is equal to 200 Hz. A rather high switching frequency has governed the choice for switching elements of crystal diodes possessing high operating speed and large service life.

To eliminate the reflections from non-loaded inputs of disconnected channels, all of these are loaded with 75 Ω resistors. The attenuation in the open channel of the switch makes $\sim$ 1 dB and is mainly determined by the diodes resistance losses.

After the recent control unit design improvement, new modes for the master clock pulses, viz. 0.2, 0.4 and 200 Hz, appeared. Availability of several operational modes has allowed choosing different forming time of the heliograph frame. Earlier, the 100/200 Hz frequency oscillator was synchronized by the electrical grid frequency, inasmuch as the mechanical system of line scanning of a recording device – being a facsimile receiver – was synchronously driven. Owing to implementation of a new receiver-recorder (DSP), the necessity in such an oscillator ceased to have significance. A new oscillator variant is crystal-controlled that has allowed to noticeably improve stable operation as a whole. Besides, the sum-difference unit – earlier always having permitted to form a heliogram pattern pencil beam using the N-S and E-W array signals – became quite unnecessary. At present, the DSP perfectly fulfills this function, but the equipment will be considered more comprehensively in the next section.

The beam switch and E-W array switch control pulses are formed with the frequency divider and the decoder. The fast scanning phase shifters

control pulses are formed with the frequency divider.

The control unit also comprises the display circuit to which the signals arrive from the monitoring circuits of phase shifters and switches. The monitoring and display circuits allow ones to fast determine the serviceability of these devices and quickly found and remedy the breakages.

10 DSP Application in Heliograph

It will be observed that as far back as the late nineties, the observations with the UTR-2 array were made only at six fixed frequencies. Such a situation hindered from obtaining a more comprehensive information on the recorded events, as well as resulted in an appreciable loss of advantage against multi-frequency observations. In recent years, however, the scope for the radio telescope receiver-recorder has been essentially expanded.

A standard approach in studying non-stationary random signals can be the instantaneous spectral analysis [39], which using allows one to transform the input signal into a two-dimensional (time-and-frequency) spectrogram. The very first broadband digital spectral receivers for the low-frequency radio astronomy employing the real time Fourier-analysis (DSP, Robin) were developed under the joint France-Austria project [33, 34] and successfully introduced at the NDA (France) and UTR-2 (Ukraine) radio telescopes [35]. These latter have permitted obtaining a great bulk of new results, including those in studies of the Sun, which are partially presented in papers [40, 41, 42, 43]. The further progress of digital and computer facilities, information and telecommunication technologies has allowed creation of spectral receivers with substantially improved parameters [44, 45]. In these latter, the input signal is digitized with the high-speed analog-to-digital converter (ADC), being then processed by the FPGA matrix that results in determination of the signal spectra in the time domains where the signal can be considered as quasistationary. The spectra obtained are

Table 2: The DSPZ key features.

Sampling frequency(MHz)	66
Operating frequency range(MHz)	8–32
Total number of frequency channels	8192
Frequency resolution(kHz)	4
Time resolution(s)	$0.2{\cdot}10^{-4}$ – 1
Dynamic range (dB)	117

then written as a number matrix (frequency channels – timing of the corresponding spectra origin) on the PC hard disk. The software developed provides for the graphic user interface in order to choose the data recording mode, data mapping after the respective real time transformations, as well as monitoring a number of other spectrum analyzer parameters.

At present, the DSPZ spectrum analyzer (see Fig. 8) is used as a heliograph's receiver-recorder. Its key features are presented in Table 2. It can operate in three different modes, called "Waveform", "Spectrum", and "Correlation". In the first one, the data flow from the output of one and/or two ADC channels is recorded on the PC storage device without any transformations or analysis. This is the simplest data recording method whose subsequent processing is entirely performed by the user. But in this case, an enormous data flow will be processed (or recorded). This flow makes about 264 Mb/s because the data digitization frequency is equal to 66 MHz. In the "Spectrum" mode, the window fast Fourier transform is applied. This procedure translates the scalar input signal into a two-dimensional spectrogram otherwise called a dynamic spectrum. Function is an average spectral power of the window signal,

$$\begin{aligned} P_n(t,f) &= |X_n(t,f)|^2, \\ X_n(t,f) &= \frac{1}{T}\int\limits_{t-T/2}^{t+T/2} x_n(\tau)g(\tau-t)\exp(-i2\pi f\tau)d\tau\,, \end{aligned} \qquad (10)$$

where $n = 1, 2$ is the input channel number, and $g(\tau - t)$ is the window

Figure 8: The UTR-2 DSPZ spectrum analyzers along with control and data acquisition PCs are shown.

function. The time window $T = 2^m \Delta t$ is associated with the interval between two sequential samples of the input signal Δt and the choice of number of spectral analysis channels. The data flow rate makes about 327 kb/s with the time resolution 100 ms. In this mode, the two input signals are treated separately from each other, therefore at the output we have two independent data flows, though the data lack the information about the phase of signals. The "Correlation" mode allows broader possibilities for the data analysis. Note that both in the "Spectrum" mode, as well as in the "Correlation" mode too, the spectral density matrix can be determined in the form

$$\mathbf{Z} = \begin{bmatrix} Z_{11} & Z_{12} \\ Z_{21} & Z_{22} \end{bmatrix} = \begin{bmatrix} P_1 & Z_{12} \\ Z_{21} & P_2 \end{bmatrix},$$

where $P_1, P_2 \in \mathbf{R}_+ \cup 0$ and $Z_{12}, Z_{21} \in \mathbf{C}$ mind though that it can be used completely only in the "Correlation" mode. This matrix is useful in the cross-spectrum analysis, when through the complex spectra of signals $x_{1,2}(\tau)$ their cross-spectral density is written as

$$K(t, f) = Z_{12} = \langle X_1(t, f) X_2^*(t, f) \rangle,$$

where the magnitudes $X_{1,2}(t, f)$ are calculated according to (10), symbol "$*$" means complex conjugate value, while the angular brackets denote the averaging over intervals T_i. The cross-spectrum analysis allows one to test the signals identity. Function $K(t, f)$ is complex and contains the information about the phase relationship of received signals. Therefore it is convenient to be presented exponentially as

$$K(t, f) = |K(t, f)| \exp[-j\Phi(t, f)],$$

where the absolute magnitude and phase angle are determined by the relations

$$|K(t, f)| = \sqrt{[\mathrm{Re}(K(t, f))]^2 + [\mathrm{Im}(K(t, f))]^2}, \tag{11}$$

$$\Phi(t, f) = \arctan\left(\frac{\mathrm{Im}(K(t, f))}{\mathrm{Re}(K(t, f))}\right), \tag{12}$$

and j is the imaginary unit. The real part of the cross-spectral density function $\mathrm{Re}(K(t,f)) = C(t,f)$ is called a cospectrum, and its imaginary part $\mathrm{Im}(K(t,f)) = Q(t,f)$ a quadrature spectrum. To come to the point of a cross-spectral function, suffice it to mention that the cospectrum $C(t,f)$ makes a contribution of oscillations of different frequencies to the general cross-spectrum for the zero phase shift between two signals. Meanwhile, the quadrature spectrum shows the contribution of different harmonics into the general cross-spectrum, when the harmonics of the first signal $x_1(\tau)$ are late for a quarter of period with respect to the corresponding harmonics of the second signal $x_2(\tau)$. In observations at the UTR-2 array, one input of DSPZ is fed with the N-S antenna signal, while the other one with the E-W one, that allows to eventually shape a pencil-beam antenna pattern for the heliograph.

The "Correlation" mode possesses yet not two data flows as the output ones, as in the "Spectrum" mode, but now four: the power spectra of each channel, and also real (cospectrum) and imaginary (quadrature spectrum) parts of a cross-spectrum. These may allow finding the coherence function which value varies from 0 (absolutely different signals) to 1 (signals are identical). That is the reason why the data flow rate increases twice in this case. During summer observations of 2009, and partially in 2010, the heliograph was employed first in the "Spectrum" mode. The DSPZ inputs were fed with the sum-difference signal. However such a data recording method is prone to appreciable loss of information on the power spectra in separate antennas and signal phase. Thereby, at summer-end of 2010, the heliograph configuration was changed, and the signal after switchboards of N-S and E-W arrays entered the corresponding DSPZ channels, without the sum-difference unit. In such a situation it is expedient to record the data using the "Correlation" mode due to its aforesaid advantages and possibility of frequency channels averaging in case of necessity.

So, in the present heliograph configuration with sequential formation

and recording of picture elements, the two ADC inputs of the DSPZ unit are fed with the outputs of N-S and E-W arrays. The N-S array has five outputs which correspond to five beams. These outputs are sequentially connected to the receiver-recorder (DSPZ) input. In the end of each cycle of beam inquiry, the auxiliary noise generator is connected in place of antenna to the both inputs of the receiver-recorder to form the separating tracks (markers) on heliograms.

The heliograph receiver-recorder functions as an amplifier and filter of received signals, shapes the array pencil-beam pattern and performs raster display in the scan region.

11 Observation Examples

In the course of the last decade, the heliographic observations with the UTR-2 array were largely made occasionally, rather for testing this instrument subjected to upgrading. The observation results have allowed to ascertain the first priority in improvement of the hardware and the software heliograph parts. Thereto, the indicated period has observed a high solar activity, and the principal problem in solar observations was radiospectroscopic research of solar burst activity at decameter wavelengths (see e.g. [40, 42, 43]).

Summarizing of the upgrading can be referred to observations in summer of 2010, which results we are going to present in this Section. These researches have included night observations of sky radio sources 3C144 (Crab Nebula), 3C274 (Virgo), 3C405 (Cygnus), etc. For our heliograph, they are considered as point sources of radio emission. Besides, they have different intensity at decameter wavelengths and may permit to estimate the heliograph sensitivity as a whole. The source tracking rate was taken equal to 16 min. For this time, the source traversed the heliogram frame from its one edge to the other. The switching rate of the fast scan phase

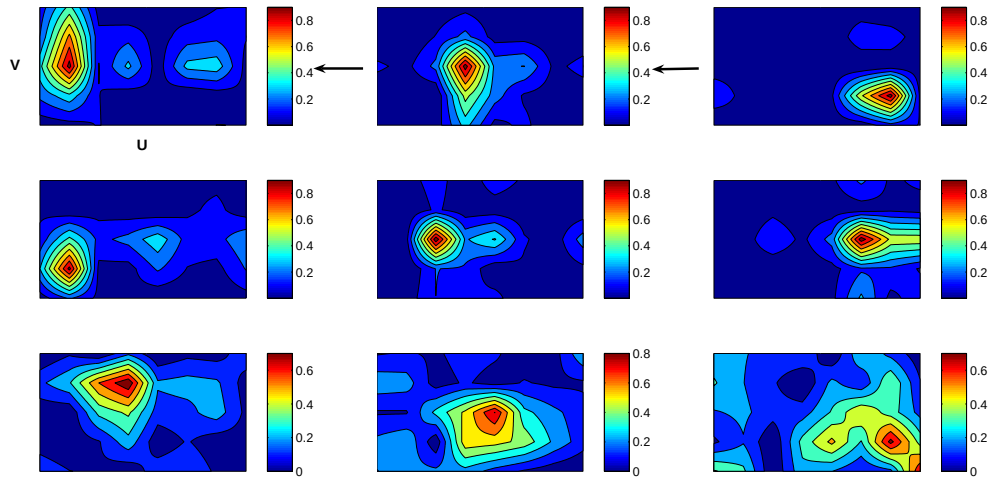

Figure 9: "Raw" (dirty) maps of sources 3C123 (upper row), 3C348 (middle) and solar corona (lower row) at $\sim$ 21 MHz. Three images show the sources motion observed owing to the celestial sphere diurnal rotation (from right to left). The images carry the UTR-2 sidelobes contribution. The radiation intensity is normalized to unit, the background is subtracted (i. e. being zero). The dark red color corresponds to maximum intensity, while the dark blue to minimum.

shifter was taken such that the heliograph image was formed for 2 min. This is quite enough for the considered case, when the changes in source position are largely caused by the celestial sphere's diurnal motion. Such an image formation rate and source tracking time have permitted us to observe the source passage from one beam of a frame to the neighbor beam in the next frame, thus showing the source crossing the whole frame (see Fig. 9, upper and middle rows), consisting, as we remember, of 5-beam eight positions. In the DSPZ "Correlation" mode, for each position in the heliograph frame we have succeeded in formation the pencil-beam pattern.

After successful observations of the aforesaid radio sources, the similar mode was applied for the quiet Sun observations, too. These latter were

made in the late August and early September, 2010. For the decameter range heliograph, the solar corona appears to be an extended source of radio emission. Therefore on the heliogram, the source will be "distributed" over several pixels. Remind that the whole image of the heliograph scan region consists of elements (or pixels). One of the major tasks implied by the heliograph application consists in observations of 2D distributions of the undisturbed Sun's corona brightness. As is known, the 11-year solar minimum occurred in 2008, therefore the quiet Sun power flux densities can be measured in the years near the solar minimum. The examples of solar corona images obtained during observations from August 28 till September 3, 2010 are shown in the lower row of images in Fig. 9, which were recorded on August 29 at $\sim$ 7:20 UT. Here, for now, shown are merely the "raw" (or dirty) maps (due to the UTR-2 pattern sidelobes contribution), but they clearly reveal the corona (or its brightest part) transition across the heliograph frame due to the celestial sphere's diurnal motion, that suggests a sufficient instrument sensitivity even for a single frequency channel. This important result highly encourages and stimulates further observations of the solar corona with the UTR-2 array based heliograph.

The here-shown presentation of observations made with the heliograph has only a demonstrational (preliminary) character. The formation of solar corona images using the data of the said observations at decameter wavelengths with their calibration, "cleaning" of images and comparison with the solar events occurred, anticipate our further efforts to end up being a separate paper.

12 Conclusions

This paper considers a functional scheme of the decameter wavelength heliograph. The heliograph is based on the UTR-2 antenna system. Any radio source is slowly tracked by the UTR-2 radio telescope standard hardware

facility. Within the heliograph field of view, this antenna pattern beam is guided by a specially designed phase shifter. The heliograph is recording the image with the sequential signal injection in each position of the pencil beam of the UTR-2 array out of its 40 positions available in a separate frame of the heliograph. The heliograph image repetition rate can be taken both rather large (suitable for analyzing the spatial characteristics of fast solar bursts), and a small one (convenient for the quiet Sun upper corona research).

The image repetition rate, owing to the motion of a five-beam set of the UTR-2 array within the heliograph scanned area, should be much greater than the Sun tracking rate. The UTR-2 phasing system cannot ensure the beam position change with such a speed since it uses the electromagnetic relays as the switched elements. That is why the UTR-2 phasing system is used only for the Sun position tracking. For fast scanning the scan sector, the UTR-2 phasing system comprises additional phase shifters possessing a fairly high operating speed and long lifetime. As the scanning is performed within small angles, the optimum alternative will be enabling the additional phase shifters between the section outputs and appropriate inputs of the E-W antenna sections phasing system. In this case, at fast scanning, the section pattern position remains the same, and the array beam moves within the section beam pattern width owing to the additional phase shifters. This results in lower received-signal intensity of the source situated near the scan sector edge due to signal strength depression on the section pattern slopes. In recorded-data processing this fact should be taken into account, and the respective corrections made in processing the observation results.

The design features of the decameter wavelength heliograph based on the UTR-2 array are such that we may belong it to the unique radio astronomy instruments. Here, suffice it to mention that among all heliographs used world-wide, this one operates the lowest frequencies for the study of cosmic

radio emission. Secondly, it is superbroad-band covering practically the entire range within 10 to 30 MHz. Thirdly, its sensitivity, time and frequency resolutions, dynamic range, signal space selection are record-breaking for the given frequency range, and consequently the problems which can be solved with this instrument have no world counterparts. The heliograph is also unique in its capability of obtaining quiet Sun's corona images for about 1 s period at distances from two to three solar radii, counted from the Sun's center, and practically without skipping in the (U, V)-plane. The heliograph's sensitivity allows observation of space-time evolution of low-contrast formations (fine structure of radio bursts, fibrous structure of Type II bursts, etc.). Besides, its dynamic range makes it possible to observe the details simultaneously with the bright radio events (strong Type III bursts, or against the background of Type II and IV bursts). The instrument has undergone a long-continued development, and in retrospect we may think with absolute certainty that the state-of-the-art heliograph performances have justified the expended energies.

13 Acknowledgements

The authors are very grateful to V. V. Zakharenko for his useful remarks and discussion of our results, to S. V. Stepkin and V. L. Kolyadin for the useful pieces of advice, to V. V. Dorovskyy for the help in accomplishment of this work.

References

[1] Krüger A. Introduction to Solar Radio Astronomy and Radio Physics. - Berlin: Springer, 1979. - 356 p.

[2] Nakajima H., Nishio M., Enome S., Shibasaki K., Takano T., Hanaoka Y., Torii C., Sekiguchi H., Bushimata T., Kawashima S.

New Nobeyama radioheliograph // J. Astrophys. Astron. - 1995. - Vol. 16, Suppl. - P. 437-442.

[3] Bogod V. M., Gel'freykh G. B., Grebinskii A. S., and Opeykina L. V. Correlation radioheliograph based on the RATAN-600 radio telescope // Radiophys. Quantum Electron. - 1996. - Vol. 39, issue 5. - P. 353-359 (translated with Izv. VUZ. Radiofiz. - 1995. - Vol. 39(5). - P. 527-537).

[4] Grechnev V.V., Lesovoi S.V., Smolkov G.Ya., Krissinel B.B., Zandanov V.G., Altyntsev A.T., Kardapolova N.N., Sergeev R.Y., Uralov A.M., Maksimov V.P., Lubyshev B.I. The Siberian solar radio telescope: the current state of the instrument, observations, and data // Solar Phys. - 2003. - Vol. 216, 1. - P. 239-272.

[5] Padin S., Scott S. L., Woody D.P., Scoville N.Z., Seling T.V., Finch R.P., Giovanine C.J., Lawrence R.P. The Owens Valley Millimeter Array // Astron. Soc. Pacif., Publ. - 1991. - Vol. 103. - P. 461-467.

[6] Yan Y., Zhang J., Chen Z., Ji G., Wang W., Liu F. Progress on Chinese solar radioheliograph in cm-dm wavebands // Astron. Res. Techn. Publ. of Nat. Astron. Observ. of China. - 2006. - Vol. 3, 2. - P. 91-98.

[7] Nancy Radio Heliograph group. The Nancay multifrequency radioheliograph: new developments and data acquisition for the solar physics community // Adv. Space Res. - 1993. - Vol. 13, 9. - P. 411-414.

[8] Ramesh R., Subramanian K.R., Sundrajan M.S., Sastry Ch.V. The Gauribidanur radioheliograph // Solar Phys. - 1998. - Vol. 181. - P. 439-453.

[9] Sheridan K.V., Labrum N.R., Payten W.J., Nelson G.J., Hill E.R. Preliminary observations of solar radio sources with the Culgoora radioheliograph operating at four frequencies // Solar Phys. - 1983. - Vol. 83. - P. 167-177.

[10] Erickson W.C., Mahoney M.J., Erb K. The Clark Lake Teepee-Tee telescope // Astrophys. J., Suppl. Series. - 1982. - Vol. 50. - P. 403-419.

[11] Lecacheux A. The Nancay Decameter Array: A useful step towards giant new generation radio telescopes for long wavelength radio astronomy: in Radio Astronomy at Long Wavelengths / Geophysical Monograph 119. Copyright by the American Geophysical Union. - 2000. - P. 321328.

[12] White S.M., Kassim N.E., Erickson W.C. Solar radioastronomy with the LOFAR (LOw Frequency ARray) radio telescope // Proc. SPIE. - 2002. - Vol. 4853. - P. 111-120.

[13] Reich W. LOFAR in Germany // Adv. Radio Sci. - 2007. - Vol. 5. - P. 407-412.

[14] Kassim N.E., Polisensky E.J. The Legacy of Clark Lake and the Road to the Long Wavelength Array // ASP Conf. Ser. - 2005. - Vol. 345. - P. 114-124.

[15] Pick M., Vilmer N. Sixty-five years of solar radioastronomy: flares, coronal mass ejections and Sun-Earth connection // Astron. Astrophys. Rev. - 2008. - Vol. 16. - P. 1-153.

[16] Abranin E.P., Baselyan L.L., Goncharov N.Yu., Zaitsev V.V., Zinichev V.A., Rapoport V.O., Tsybko Ya.G. Angular sizes of striaburst sources in the range 24-26 MHz // Solar Phys. - 1978. - Vol. 57. - P. 229-235.

[17] Ellis G.R.A., McCulloch P.M. Frequency splitting of solar radio bursts // Austr. J. of Phys. - 1967. - Vol. 20. - P. 583-594.

[18] Abranin E.P., Baselyan L.L., Goncharov N.Yu., Zaitsev V.V., Zinichev V.A., Rapoport V.O., Tsybko Ya.G. Positions of solar storm burst sources by observations with a heliograph based on the UTR-2 antenna at 25 MHz // Solar Phys. - 1980. - Vol. 66. - P. 393-409.

[19] Malinge A.-M. Relation entre les oranges radioelectriques solaires et les eruptions chromospheriques // Ann. Astrophys. - 1960. - Vol. 23. - P. 574-584.

[20] Clavelier B. Sur quelques caracteristiques des sursauts de type IV. I // Ann. Astrophys. - 1968. - Vol. 31. - P. 445-455.

[21] Gergely T. E., Kundu M. R. Decameter storm radiation, II // Solar Phys. - 1975. - Vol. 41. - P. 163-188.

[22] Abranin E.P., Baselyan L.L., Zaitsev V.V., Rapoport V.O., Tsybko Ya.G. Radio echo and sporadic scattering in the solar corona // Solar Phys. - 1982. - Vol. 78. - P. 179-186.

[23] Abranin E.P., Baselyan L.L., Zaitsev V.V., Rapoport V.O., Tsybko Ya.G. Multiple radio echoes in the solar corona // Solar Phys. - 1984. - Vol. 91. - P. 383-398.

[24] Abranin E. P., Baselyan L. L., and Tsybko Y. G. Dynamic spectrum parameters of the solar decameter type IIId radio bursts with echo components // Astron. Rep. - 1996. - Vol. 40, issue 6. - P.853-859 (translated with Astron. Zh. - 1996. - Vol. 73(6). - P. 939-946).

[25] Abranin E. P., Baselyan L. L., and Tsybko. Y. G. Quasi-periodic structure of solar type IIId radio bursts with echo components //

Radiophys. Quantum Electron. - 1997. - Vol. 40, issue 9. - P. 720-727 (translated with Izv. VUZ. Radiofiz. - 1997. - Vol. 40(9). - P. 1073-1085).

[26] Abranin E. P., Baselyan L. L., and Tsybko Y. G. Preliminary data on decameter type IIId bursts with echo components obtained from a two-dimensional radio heliograph // Radiophys. Quantum Electron. - 1998. - Vol. 41, issue 1. - P. 68-77 (translated with Izv. VUZ. Radiofiz. - 1998. - Vol. 41(1). - P. 105-120).

[27] Abranin E. P., Baselyan L. L., and Tsybko Y. G. A new spectral form of decameter type IIId radio bursts. Observations of superluminal sources of narrow-band radio emission in the solar vicinity // Radiophys. Quantum Electron. - 1999. - Vol. 42, issue 5. - P. 357-369 (translated with Izv. VUZ. Radiofiz. - 1999. - Vol. 42(5). - P. 403-417).

[28] Abranin E. P., Baselyan L. L., and Tsybko Y. G. Amplitude profiles of solar type IIId radio bursts with echo components and the global dislocation of their elementary quasi-monochromatic sources // Radiophys. Quantum Electron. - 2000. - Vol. 43, issue 12. - P. 923-937 (translated with Izv. VUZ. Radiofiz. - 2000. - Vol. 43(12). - P. 1027-1043).

[29] Gergely A.C. On the observation of scattered radio emission from sources in the solar corona // Solar Phys. - 1974. - Vol. 35. - P. 153-169.

[30] Afanasiev A.N. Mathematical modeling of the formation of type IIId solar decameter radio bursts with echo components // Solar Phys. - 2006. - Vol. 238. - P. 87-104.

[31] Stepanova N.A., Baselyan L.L., Abranin E.P., Brazhenko A.I., Sapogov S.A., Tsybko Ya.G. Decameter solar type III bursts: data

classification with use of cluster analysis // Solar Phys. - 1995. - Vol. 156, issue 1. - P. 131-143.

[32] Abranin E. P., Bruck Yu. M., Zakharenko V. V., Konovalenko A. A. The New Preamplification System for the UTR-2 Radio Telescope // Exper. Astron. - 2001. - Vol. 11, issue 2. - P. 85-112.

[33] Kleewein P., Rosolen C., Lecacheux A. New Digital Spectrometers for Ground-Based Decameter Radio Astronomy: in Planetary Radio Emissions 1V / Edited by H.O. Rucker, S.J. Bauer A., and Lecacheux A. - Austrian Academy of Sciences Press, Vienna, 1997. - P. 349-357.

[34] Lecacheux A., Rosolen C., Clerc V., Kleewein P., Rucker H.O., Boudjada M.Y., W. Van Diel. Digital techniques for ground-based low frequency radioastronomy // Proc. SPIE 3357. - 1998. - P. 533-542.

[35] Lecacheux A., Konovalenko A.A., Rucker H.O. Using Large radio telescope at decameter wavelength // Planet. Space Sci. - 2004. - Vol. 52. - P. 1357-1374.

[36] Braude S. Ya., Men A. V., Sodin L. G. The UTR-2 decametric-wave radio telescope // Antenny. - 1978, no. 26. - P. 3-15 (in Russian).

[37] Men A. V., Sodin L. G., Sharykin N. K., Bruk Yu. M., Melianovskii P. A., Iniutin G. A., Goncharov N. Yu. Design principles and characteristics of the antennas of the UTR-2 radio telescope. - Antenny. - 1978, no. 26. - P. 15-57 (in Russian).

[38] Bruk Y. M., Inyutin G. A. Binary-discrete delay lines (phase shifters) for broadband electrically steered antennas // Antenny. - 1978, no. 26. - P. 107-121 (in Russian).

[39] Bendat J. S., Piersol A. G. Random data: Analysis and measurement procedures. - 2nd ed. - New York: John Wiley, 1986. - 566 p.

[40] Mel'nik V.N., Konovalenko A.A., Rucker H.O., tanilavky A.A., Abranin E.P., Lecacheux A., ann G., Warmuth A., Zaitev V.V., Boudjada . Y., Dorovkii V.V., Zaharenko V.V., Liachenko V.N., Roolen C. Observations of solar type II bursts at frequencies 10-30 MHz // Solar Phys. - 2004. - Vol. 222. - P. 151-166.

[41] Melnik V. N., Konovalenko A. A., Dorovskyy V. V., Rucker H. O., Abranin E. P., Lisachenko V. N., Lecacheux A. Solar drift pair bursts in the decameter range // Solar Phys. - 2005. - Vol. 231. - P. 143-155.

[42] Chernov G. P., Stanislavsky A. A., Konovalenko A. A., Abranin E. P., Dorovsky V. V., and Rucker H.O. Fine structure of decametric type II radio bursts // Astron. Lett. - 2007. - Vol. 33, issue 3. - P. 192-202 (translated with Pis'ma v Astron. Zh. - 2007. - Vol. 33(3). - P. 221-232).

[43] Konovalenko A.A., Stanislavsky A.A., Abranin E.P., Dorovsky V.V., Melnik V.N., Kaiser M.L., Lecacheux A., Rucker H.O. Absorption in Burst Emission // Solar Phys. - 2007. - Vol. 245. - P. 345-354.

[44] Kozhin R.V., Vinogradov V.V., Vavriv D.M. Low-noise, high dynamic range digital receiver/spectrometer for radio astronomy applications // MSMW Symp. Proc. - Kharkov (Ukraine). - 2007. - P. 736-738.

[45] Ryabov V.B., Vavriv D.M., Zarka P., Ryabov B.P., Kozhin R., Vinogradov V.V., Denis L. A low-noise, high-dynamic-range, digital receiver for radio astronomy applications: an efficient solution

for observing radio-bursts from Jupiter, the Sun, pulsars, and other astrophysical plasmas below 30 MHz // Astron. Astrophys. - 2010. - Vol. 510. - P. 16-28.